NeuroImage: Clinical 1 (2012) 57–65

Contents lists available at ScienceDirect

NeuroImage: Clinical

journal homepage: www.elsevier.com/locate/ynicl

Abnormalities in the brain of streptozotocin-induced type 1 diabetic rats revealed by diffusion tensor imaging ☆

Mingming Huang [a,b,1], Lifeng Gao [a,b,1], Liqin Yang [a,b], Fuchun Lin [a], Hao Lei [a,*]

[a] Wuhan Center for Magnetic Resonance, State Key Laboratory of Magnetic Resonance and Atomic and Molecular Physics, Wuhan Institute of Physics and Mathematics, Chinese Academy of Sciences, Wuhan, China
[b] Graduate School, Chinese Academy of Sciences, Beijing, China

ARTICLE INFO

Article history:
Received 27 June 2012
Received in revised form 1 September 2012
Accepted 5 September 2012
Available online 14 September 2012

ABSTRACT

Diabetes mellitus affects the brain. Both type 1 and type 2 diabetic patients are associated with white matter (WM) damage observable to diffusion tensor imaging (DTI). The underlying histopathological mechanisms, however, are poorly understood. The objectives of this study are 1) to determine whether streptozotocin (STZ)-induced type 1 diabetes is associated with WM damage observable to DTI; and 2) to understand the pathophysiological aspects underlying STZ-induced brain injuries. Male Sprague–Dawley rats received a single intraperitoneal injection of STZ (62 mg/kg). DTI was used to assess brain abnormalities at 4 weeks after induction, combined with histological assessments and ultrastructural analysis. Compared to controls, the STZ-induced rats showed significantly reduced fractional anisotropy (FA) in the motor/somatosensory cortex and striatum. Histologically, the cortex and striatum of the diabetic animals are characterized by demyelination and axonal degradation. In conclusion, STZ-induced diabetes is associated with striatal/cortical injuries observable to DTI. The DTI abnormalities are likely manifestations of demyelination and axonal degradation in the affected brain regions, and can potentially be used as surrogates for evaluating diabetic brain injuries.

Introduction

Patients with diabetes mellitus, and in particular those with poor glycemic control, often experience brain complications (van Harten et al., 2006). It is well known that long-standing diabetes increases the risk of brain atrophy, lacunar infarcts and white matter (WM) lesions. The functional/behavioral consequences of diabetic brain complications include cognitive dysfunction and movement disorders (Shan et al., 1998; van Elderen et al., 2010; van Harten et al., 2006).

Diffusion tensor imaging (DTI) is a magnetic resonance imaging (MRI) technique that has been increasingly used in the diagnosis and prognosis of WM diseases (Tournier et al., 2011). Parametric diffusion indices derived from DTI, such as fractional anisotropy (FA) and directional diffusivity are often used to assess microstructural changes of brain tissues (Tournier et al., 2011).

Only few previous studies have assessed WM damage in diabetic patients with DTI. It was shown that patients with long-standing type 1 diabetes had significantly reduced FA in the posterior corona radiata and optic radiation, which correlated with the duration of diabetes (Kodl et al., 2008). These patients also had significantly reduced cortical thickness in brain regions with high connectivity to the injured WM tracts (Franc et al., 2011). DTI assessment among individuals with type 2 diabetes demonstrated diffuse but predominantly frontal and temporal WM microstructural abnormalities (Yau et al., 2009). A more recent DTI study found that, compared to the control, type 2 diabetic patients had significantly increased mean diffusivity (MD) of the brain parenchyma and significantly decreased FA in the bilateral frontal WM (Hsu et al., 2012). They further showed that there was a significant association between disease duration and microstructural properties in the bilateral cerebellum, temporal lobe WM, right caudate and bilateral cingulate gyrus (Hsu et al., 2012).

In a mouse model of streptozotocin (STZ)-induced type 1 diabetes, WM changes and brain atrophy were detected 8 months after induction (Francis et al., 2008). Yang et al. showed that T_2-weighted and magnetization transfer MRI can be used to assess WM abnormalities in rats with type 1 diabetes or type 2 diabetes, and the changes of MRI signal intensity are associated with loss of myelin proteins and oligodendroglia (Yang et al., 2011).

In this study, we used DTI to assess brain abnormalities in a rat model of STZ-induced type 1 diabetes at 4 weeks after induction. The imaging results were correlated to those of histological assessments and ultrastructural analysis. The main purposes of the study are 1) to determine, without glycemic control, whether STZ-induced type 1 diabetes can

* Corresponding author at: Wuhan Institute of Physics and Mathematics, Chinese Academy of Sciences, 30# Xiaohongshan, Wuhan, Hubei 430071, China. Tel.: +86 27 87198542; fax: +86 27 87199291.
E-mail address: leihao@wipm.ac.cn (H. Lei).

[1] Mingming Huang and Lifeng Gao contributed equally.

2213-1582/$ – see front matter © 2012 The Authors. Published by Elsevier Inc. All rights reserved.
http://dx.doi.org/10.1016/j.nicl.2012.09.004

induce WM damage observable to DTI; and 2) to understand the pathophysiological aspects underlying STZ-induced brain injuries.

Materials and methods

Animals

All animal protocols were approved by the Institutional Animal Care and Use Committee. Forty male Sprague–Dawley rats, about 10 weeks old and weighing about 300 g, were obtained from the Experimental Animal Center, Wuhan University. Type 1 diabetes (n = 24) was induced by a single intraperitoneal injection of streptozotocin (62 mg/kg) (Sigma, St. Louis, MO) dissolved in 0.01 mol/L citric acid solution (pH = 4.5). The control animals (n = 16) were injected with the same amount of solvent. The animals were then housed individually in a temperature- and humidity-controlled environment on a 12-h light/dark cycle. To prevent hypoglycemia, the STZ-induced rats were allowed to have free access to D5W (water with 5% dextrose) during the first 24 h after STZ injection. Three days after the induction, fasting blood glucose levels and body weights were measured. Six STZ-induced rats that had a fasting blood glucose level less than 13.5 mmol/L were excluded. Fasting blood glucose level and body weight were measured weekly for the next 4 weeks.

MRI acquisition

All magnetic resonance experiments were performed on a 7 T/20-cm-diameter bore Bruker Biospec scanner at 4 weeks after STZ induction. A volume coil was used for radiofrequency transmission, and a quadrature surface coil for signal detection. DTI was performed with a 4-shot spin-echo echo planar imaging sequence, an encoding scheme of 30 gradient directions homogenously distributed on the unit sphere and the following parameters: repetition time (TR) 5000 ms, echo time (TE) 26 ms, field of view (FOV) 3 cm × 3 cm, slice thickness 0.8 mm, matrix size 128 × 128, Δ 14 ms, δ 3 ms, two b values of 0 and 800 s/mm^2 and 4 averages. The animals were anesthetized by 1.5–2% isoflurane in pure O_2 delivered via a nose cone during the imaging sessions.

Histology and immunohistochemistry

After being imaged, three randomly selected rats from each group were anesthetized with an overdose of 5% chloral hydrate, and perfused transcardially with 0.9% saline and 4% paraformaldehyde in phosphate-buffered solution (PBS). The brains were immediately removed and postfixed in the same fixative at 4 °C until being sectioned on a cryostat (Leica, Germany). Coronal brain sections 10 μm-thick were obtained and stored at −20 °C until use.

Bielschowsky's sliver (BS) staining was used to assess the morphology and integrity of axons and neuropil. The brain sections were washed with distilled water and incubated in 10% silver nitrate solution for 35–40 min at room temperature. The sections were then processed sequentially with a 5% methanal solution for 5 min, a 10% ethanol solution for 2 min, a silver amino solution for 2 min and a 10% methanal solution for 5 min, followed by washes with distilled water and dehydration in 100% ethanol.

Klüver–Barrera (KB) staining was used for demonstrating the existence of myelin. The brain sections were incubated with a 0.1% Luxol fast blue (LFB) solution at 60 °C overnight and rinsed with a 95% ethanol solution and distilled water. The brain sections were then immersed in a 0.05% lithium carbonate solution for 1 min and a 70% ethanol solution for 2 min, and treated with 0.1% cresyl violet and rinsed with 95% ethanol. Finally, the sections were dehydrated in 100% ethanol, cleared with xylene and mounted.

Nissl staining was used to assess neuronal damage in the cortex. The brain sections were incubated with a 5% toluidine blue solution at room temperature for 15 min. Following rinses with tap water, the sections were dehydrated and mounted.

Diminution in neurofilament immunostaining of SMI-31 is usually considered a sign of axonal degeneration (Budde et al., 2007). For SMI-31 immunohistochemistry, the brain sections were pre-incubated with a 0.01 M citrate buffer (pH 6.0) at 80–85 °C for about 10 min, until the temperature of the antigen retrieval solution had reached room temperature. After a brief wash in 0.01 M PBS, the brain sections were incubated in 0.2% Triton X-100 at 37 °C for 30 min, washed in 0.01 M PBS and then incubated with 10% normal goat serum at 37 °C for 40 min. Subsequently, the brain sections were incubated in anti-phosphorylated neurofilaments SMI-31 antibody (diluted 1:1000 in PBS; Sternberger Monoclonals Lutherville, Maryland) at 37 °C for 1 h and then at 4 °C for additional 21 h. Further washes with 0.01 M PBS were performed before incubation in Alexa 488-rabbit anti-goat IgG antibody (diluted 1:200 in 0.01 M PBS) at 37 °C for 1 h. The sections were washed with 0.01 M PBS and dehydrated before being mounted.

Methylene blue staining was used for morphometric analysis of myelinated axons. Transmission electron microscopy was used for ultrastructural assessments of myelin integrity and axonal injuries. Samples from the striatum and cortex were collected and fixed with 2.5 wt.% glutaraldehyde dissolved in 0.01 M PBS (pH 7.4). The samples were postfixed with 1% osmium tetroxide, dehydrated, embedded in resin and sectioned to 80 nm- or 1 μm-thick slices. The 1 μm-thick slices were stained with methylene blue. The 80 nm-thick slices were stained with uranyl acetate and lead citrate for ultrastructural tissue examination under an H-7000FA transmission electron microscope (Hitachi, Japan).

Image pre-processing

The DTI data from two rats in the STZ-induced group were excluded because of poor image quality. As a result, the DTI data from a total of sixteen rats in the STZ group and sixteen rats in the control group were included in the final analysis. For each animal, the FMRIB's Diffusion Toolbox in FSL (http://www.fmrib.ox.ac.uk/fsl) was used to realign diffusion-weighted images to corresponding non-diffusion-weighted (b = 0) images with an affine transformation to minimize image distortion due to eddy currents. The diffusion tensor for each voxel was estimated by a multivariate linear fitting algorithm, and then diagonalized to obtain its eigenvalues (λ_1, λ_2, λ_3). The voxel-wise values of FA, axial diffusivity (λ_1, D_a) and radial diffusivity ($(\lambda_2+\lambda_3)/2$, D_r) were calculated. Residual maps were calculated as previously described to evaluate the accuracy of tensor fitting (Tournier et al., 2011).

Voxel-based analysis of DTI data

Voxel-based analysis (VBA) of FA data was performed using statistical parametric mapping (SPM8, http://www.fil.ion.ucl.ac.uk/spm/). The following processing schemes were used: (1) creating population-specific template. First, the b = 0 image of one representative control rat was trilinearly interpolated into an isotropic voxel size of 0.117 mm^3 and used as the initial template. Then the b = 0 images of all the other (including control and STZ-induced) animals were co-registered to this initial template using affine transformation. A population-specific template was then created by averaging the normalized images; (2) VBA on FA. The b = 0 image of each rat was co-registered to the population-specific template using affine transformation. For each individual animal, the same transformation matrix was applied to normalize the FA maps spatially. All normalized FA images were then smoothed with an isotropic 0.351-mm (3 times the dimension of the isotropic voxel after interpolation) full width at half maximum (FWHM) Gaussian kernel to reduce the effect of misregistration in spatial normalization. The normalized and smoothed FA images were then analyzed voxel-wise by SPM8 within the framework of general linear model. Only the pixels where all rats had a FA value greater than 0.15 were analyzed. This empirical cut-off value was used to eliminate fictitious results arising

from inter-subject variations and in the voxels with a low probability of being WM, such as the CSF voxels (Hugenschmidt et al., 2008). The t maps were thresholded using a confidence level of $p<0.005$ ($t>3$) and an extent cluster size greater than 10 contiguous voxels.

Histogram and region of interest (ROI) analysis of DTI data

The DTI changes in the striatum and cortex were further analyzed by histogram and ROI analysis as previously described (Yu et al., 2006). Masks of the bilateral striatum and cortex (Figs. 2 and 3) were derived manually from the FA template. The ROI representing bilateral striatum spanned 24 interpolated slices from Bregma 2.52 to 0. The ROI representing bilateral cortex spanned 43 interpolated slices from Bregma 3.00 to −0.60. The resulting masks were then superimposed onto the FA images of each individual animal. Histograms containing 1000 bins were created from the bilateral striatum and cortex of each rat. To compensate for variability of brain size, each bin was normalized by the total number of voxels contributing to the histogram. To reduce the possible effects of local minimum, the histograms from each rat were subjected to a 5-point median smoothing procedure. Three parameters were then derived from the smoothed histogram of each subject, including the averaged FA value, histogram peak height and histogram peak location. Group-averaged histograms were also calculated for presentation.

The striatum was composed of fiber-rich WM-like regions having high FA values and gray matter (GM)-like regions having low FA values. To pinpoint the exact locations of the diabetes-induced FA changes, we divided the ROI representing the whole striatum into two sub-ROIs based on the averaged FA map from the control group. A cutting FA value of 0.2 was used to classify each voxel within the striatal mask into either the high FA sub-ROI or the low FA sub-ROI (Smith et al., 2006). The averaged DTI indices within the sub-ROIs were calculated and compared between the control and STZ groups (Fig. 3). Similar analyses were also conducted for the cortex (Fig. 4).

Statistical analysis

Repeated measures analysis of variance (ANOVA) was used to analyze body weight and blood glucose data. Two-tailed Student's *t*-tests were used to assess the statistical significance of inter-group difference in histogram parameters and diffusion indices. The significance level was set at $p<0.05$ with Bonferroni correction for multiple comparisons.

Results

Body weight and blood glucose level

Table 1 shows the body weight and fasting blood glucose data. No statistically significant difference in body weight was found between the groups before saline/STZ treatment, nor in fasting blood glucose level. The control rats showed increasing body weight over time, while the STZ group had decreasing body weight. The fasting blood glucose level in the STZ group was significantly higher than that in the control group at 3 days and the time points after. Repeated measures ANOVA revealed that the main effects of group, time and group × time interaction were statistically significant for both body weight and fasting blood glucose level.

Voxel-based analysis of DTI data

Fig. 1A shows representative raw diffusion-weighted ($b=0$ and 800 s/mm^2) images acquired from a control animal, as well as a residual map demonstrating the accuracy of tensor fitting. The results of VBA are shown in Fig. 1B. Compared to the control animals, the diabetic rats exhibited significant decreases of FA in the bilateral striatum, motor cortex and somatosensory cortex.

Histogram/region of interest analysis of DTI data

Compared to the control group, the STZ group showed a left-shifting FA histogram in the bilateral striatum (Fig. 2A). The inter-group difference in histogram peak location (Fig. 2B) was statistically significant, but not the difference in histogram peak height (Fig. 2C). The STZ group showed significantly decreased average striatal FA, which occurred in both the GM-like regions where $FA<0.2$ and the fiber bundle-dominated region where $FA\geq0.2$ (Fig. 2D). The reduction of striatal FA in the STZ group was accompanied by a significantly decreased D_a and an unchanged D_r (Fig. 2E and F).

The group-average FA histograms of the bilateral cortex are shown in Fig. 3A. Compared to the control group, the STZ group had a significantly ($p<0.05$) higher histogram peak height (Fig. 3B), but unchanged histogram peak location (Fig. 3C). The decrease of cortical FA in the STZ group appeared to be confined to the WM-like regions where $FA\geq0.2$ (including the molecular layer and the pyramidal layers, Fig. 3D and E). The changes of FA in the regions with $FA<0.2$ (including the granular layers and part of the polymorphic layer) were not statistically significant (Fig. 3D). For the STZ group, the decrease of FA in the cortical region with $FA\geq0.2$ was accompanied by a slightly increased D_r and an unchanged D_a (Fig. 3F).

Histopathological changes in striatum

The histopathological changes of the fiber bundles in the striatum of STZ-induced rats included: less staining with LFB (Fig. 4B) and SMI-31 (Fig. 4D), and sparser/disarranged neurofibrils as revealed by BS staining (Fig. 4F). The result of both BS staining and methylene blue staining (arrows in Fig. 4H) indicated vacuole formation in the striatal fiber bundles of the STZ-induced animals. Ultrastructural analysis of the axons in the striatal fiber bundles showed signs of rarefaction of myelin sheath (arrows in Fig. 4J), myelin loss (arrowhead in Fig. 4K) and axonal degradation (asterisk in Fig. 4K).

Histopathological changes in cortex

The histopathological changes in cortex of the STZ-induced animals included rarefied neuropil in the molecular layer (Fig. 5C), dystrophic pyramidal neurons exhibiting fewer processes and poorly BS-stained somas (Fig. 5E and G), and signs of neuronal dystrophia (arrows in Fig. 5O) or loss (asterisk in Fig. 5M) in the polymorphic layer. Ultrastructural analysis showed that the pyramidal neurons of the STZ animals were associated with compromised integrity of the

Table 1
Fasting blood glucose level and body weight in control (Con) and STZ-treated animals.

		Day 0	Day 3	Day 7	Day 14	Day 28
Blood glucose (mmol/L)	Con (n = 16)	4.2 ± 0.6	5.4 ± 1.1	3.5 ± 0.5	3.4 ± 0.3	3.7 ± 0.6
	STZ (n = 16)	4.0 ± 0.5	23.6 ± 7.6*	19.0 ± 6.3*	17.3 ± 3.9*	25.9 ± 7.0*
Body weight (g)	Con (n = 16)	293.3 ± 27.5		322.2 ± 31.0	343.5 ± 30.4	387.6 ± 36.1
	STZ (n = 16)	300.7 ± 17.3		268.0 ± 21.7*	250.8 ± 31.5*	230.4 ± 30.2*

* Significantly different from the control group ($p<0.0001$, two-sample t-test).

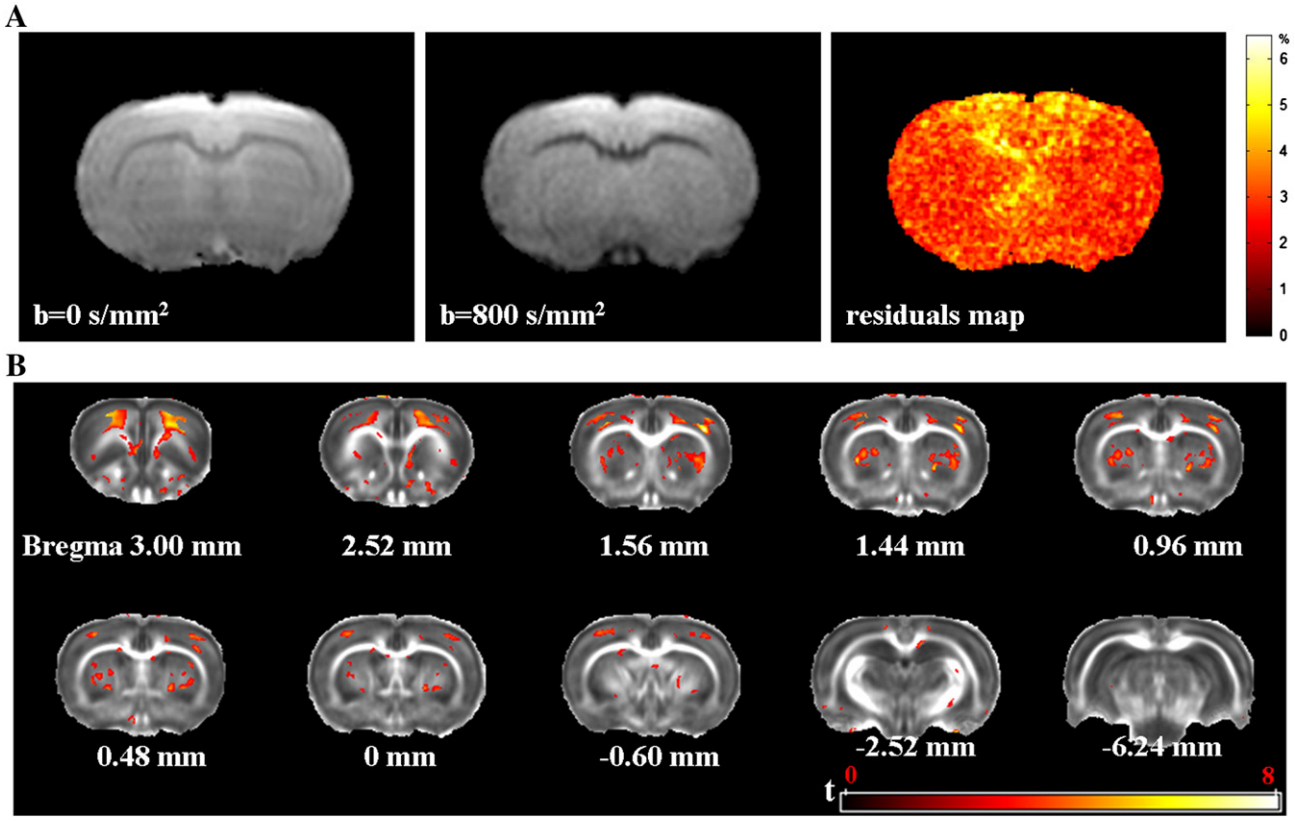

Fig. 1. Representative raw diffusion-weighted images from a control rat are shown in (A), as well as the corresponding residual map demonstrating the accuracy of tensor fitting. Panel B shows that the STZ-induced rats had diffuse reduction of FA in bilateral striatum and motor/somatosensory cortex. Pixels with statistical significance ($t > 3$, voxel extent threshold = 10) are shown in color and superimposed on the population-specific FA template generated from 16 control rats and 16 STZ-induced rats. An FA threshold of 0.15 was used when generating the t map. The color bar in (A) denotes the relative amplitude of the residuals (as percentage of the signal intensity of the corresponding pixel in the raw images). The color bar in (B) denotes t scores (range 0–8).

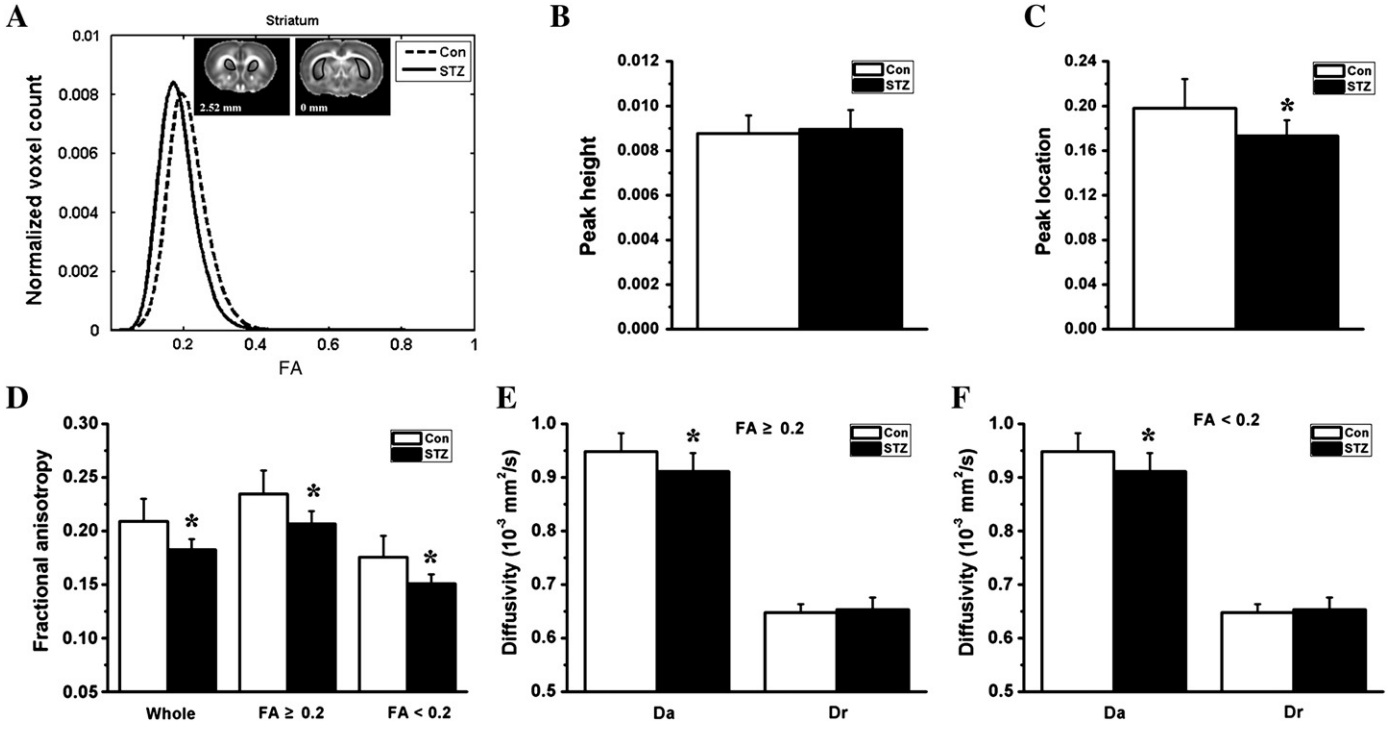

Fig. 2. Histogram and region of interest analysis of the diffusion indices in the bilateral striatum. The group-averaged FA histograms of the bilateral striatum (from Bregma 2.52 to 0 mm) are shown in the form of line graphs in A. Compared to the control group (Con), the STZ group (STZ) showed a statistically significant ($^*p < 0.001$) reduction in histogram peak location (B), but no change in histogram peak height (C). Compared to the control group, the STZ group showed significantly reduced average FA in the whole striatum, the gray matter-like region with FA < 0.2, and the white matter-like region with FA ≥ 0.2 (D, $^*p < 0.001$). The reduction of FA in the diabetic striatum was associated with a significantly decreased axial diffusivity (D_a, F and G, $^*p < 0.05$ vs. Con) and unchanged radial diffusivity (D_r).

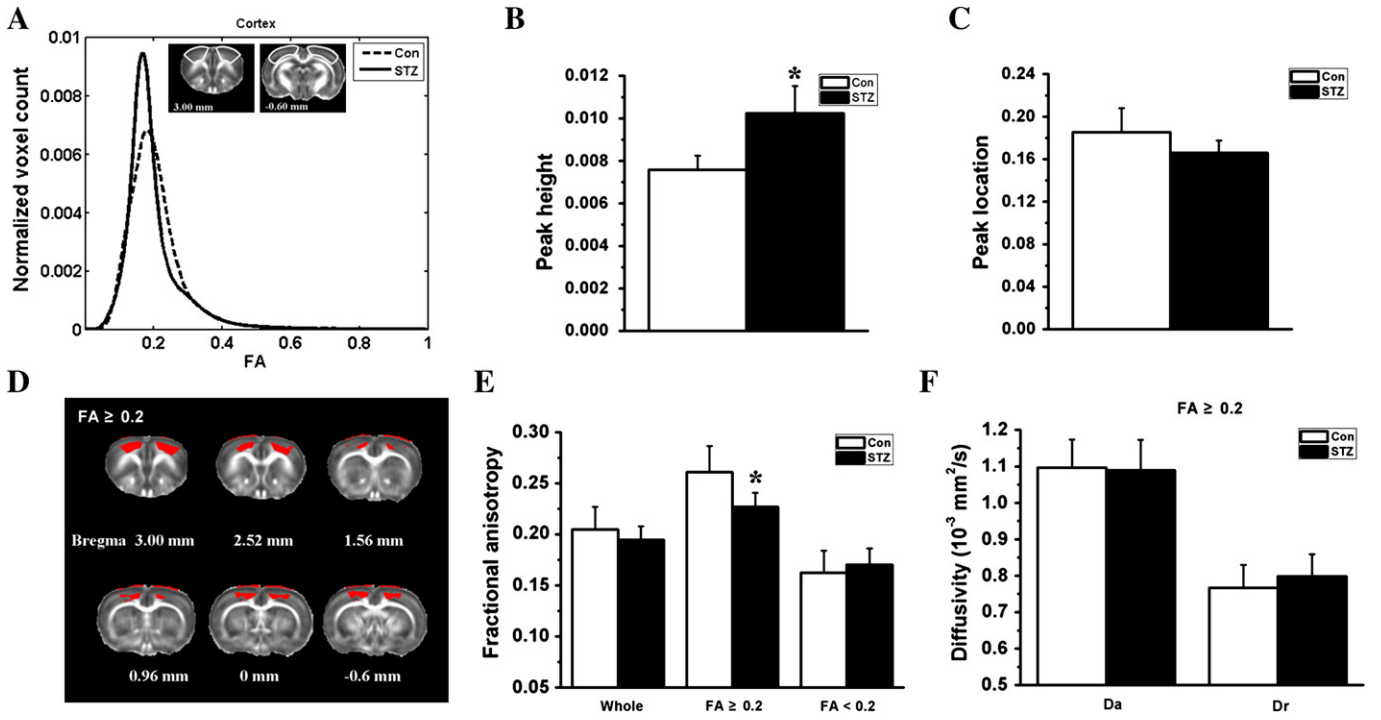

Fig. 3. Histogram and region of interest analysis of the diffusion indices in the bilateral cortex. The group-averaged FA histograms of the bilateral cortex (from Bregma 3.00 to −0.60 mm) are shown in the form of line graphs in A. Compared to the control group (Con), the STZ group (STZ) showed a statistically significant (*$p<0.05$) increase in histogram peak height (B), but no change in histogram peak location (C). The STZ group showed significantly reduced FA only in the cortical region with FA≥0.2 (D and E). Panel D shows the regions with FA≥0.2 (in red color) within the cortex mask. The FA changes in the whole cortex and cortical region with FA<0.2 (including granular layer and partly polymorphic layer) were not statistically significant (E). Panel F demonstrates that the reduction of FA in the cortical region with FA≥0.2 was associated with a slightly increased radial diffusivity (D_r) and an unchanged axial diffusivity (D_a).

myelin sheath surrounding the axons (arrows in Fig. 5I), loss and/or fragmentation of neurofilaments in the dendrites (asterisk in Fig. 5K), mitochondrial abnormalities (arrowheads in Fig. 5I and K) and aggregation of cellular organelle (circle in Fig. 5K).

Discussion

In the present study, brain injuries in a rat model of STZ-induced type 1 diabetes were evaluated with DTI. It was shown that, without glycemic control, the STZ-induced animals developed reduced FA in the striatum and motor/somatosensory cortex as early as 4 weeks after induction. Histologically, the brain regions showing FA changes were associated with demyelination, axonal degradation and neuronal dysfunction/loss.

Diabetes-induced DTI changes

Diffusion indices derived from DTI, such as FA, are widely-used surrogates for WM microstructural integrity. Clinical studies have shown that both type 1 diabetic and type 2 diabetic patients are associated with WM abnormalities observable to DTI. Lower FA values were found in the posterior corona radiata and the optic radiation of type 1 diabetic patients (Kodl et al., 2008), and in the frontal, temporal and right caudate WM of type 2 diabetic patients (Hsu et al., 2012; Yau et al., 2009).

Interestingly, we did not find any significant FA changes in the major WM tracts of diabetic animals. Instead, without glycemic control, the STZ-induced rats were shown to have significantly reduced FA in the bilateral striatum and motor/somatosensory cortex as early as 4 weeks after induction. The FA reduction in the striatum appeared to be homogenous, and accompanied by a significantly decreased D_a and a slightly increased D_r (Fig. 2). It is generally believed that the increase of D_r in WM is associated with demyelination (Song et al., 2002, 2005). In contrast, D_a appeared to be a marker more closely related to axonal damage (Sun et al., 2006). Decreased D_a has been shown to be associated with axonal degeneration (i.e., loss of phosphorylated neurofilaments) and impaired axonal transport (Deboy et al., 2007; Wu et al., 2007). Histologically, the striatal fiber bundles in our STZ-induced animals were characterized by both demyelination and axonal degeneration, consistent with the DTI findings.

The water diffusion anisotropy in the cortex mainly originates from the radial pyramidal neurons and the packed arrangement of axons (Mukherjee et al., 2002). It has also been reported that neuron density and glial activity can also modulate anisotropic diffusion of water in the cortex (Beppu et al., 2005; Neil et al., 1998). Unlike the case in the striatum, the cortical changes of FA were not homogenous, but rather confined to layers with high FA values (including the molecular layer, the pyramidal layer and part of the polymorphic layer, Figs. 1B and 3). The reduction of FA in the cortex was mainly caused by an increase in D_r, without apparent changes in D_a (Fig. 3). Interestingly, the cortical regions with FA reduction appeared to coincide with those showing axonal degradation and/or neuronal loss. For example, the neuropil in the molecular layer of the STZ-induced rat appeared to be rarefied compared to that in the control; the neurons in the pyramidal layer of the STZ-induced animals exhibited compromised integrity of the myelin sheath, damaged neurofilaments in the dendrites and mitochondrial abnormality (Fig. 5). Therefore degeneration of the pyramidal neurons could have played a significant role in causing the diffusion changes in the cortex.

However, it should be emphasized that the rat striatum and cortex are heterogenous regions in which WM and GM are mixed together. Due to the complex tissue configurations in these regions and the partial volume effects, it is the most likely that there is more than one dominant fiber orientation within a single striatal/cortical voxel. Under such circumstances, the calculation of parametric diffusion indices may not be as straightforward as that in major WM tracts, and could be affected by factors that are not necessarily related to WM

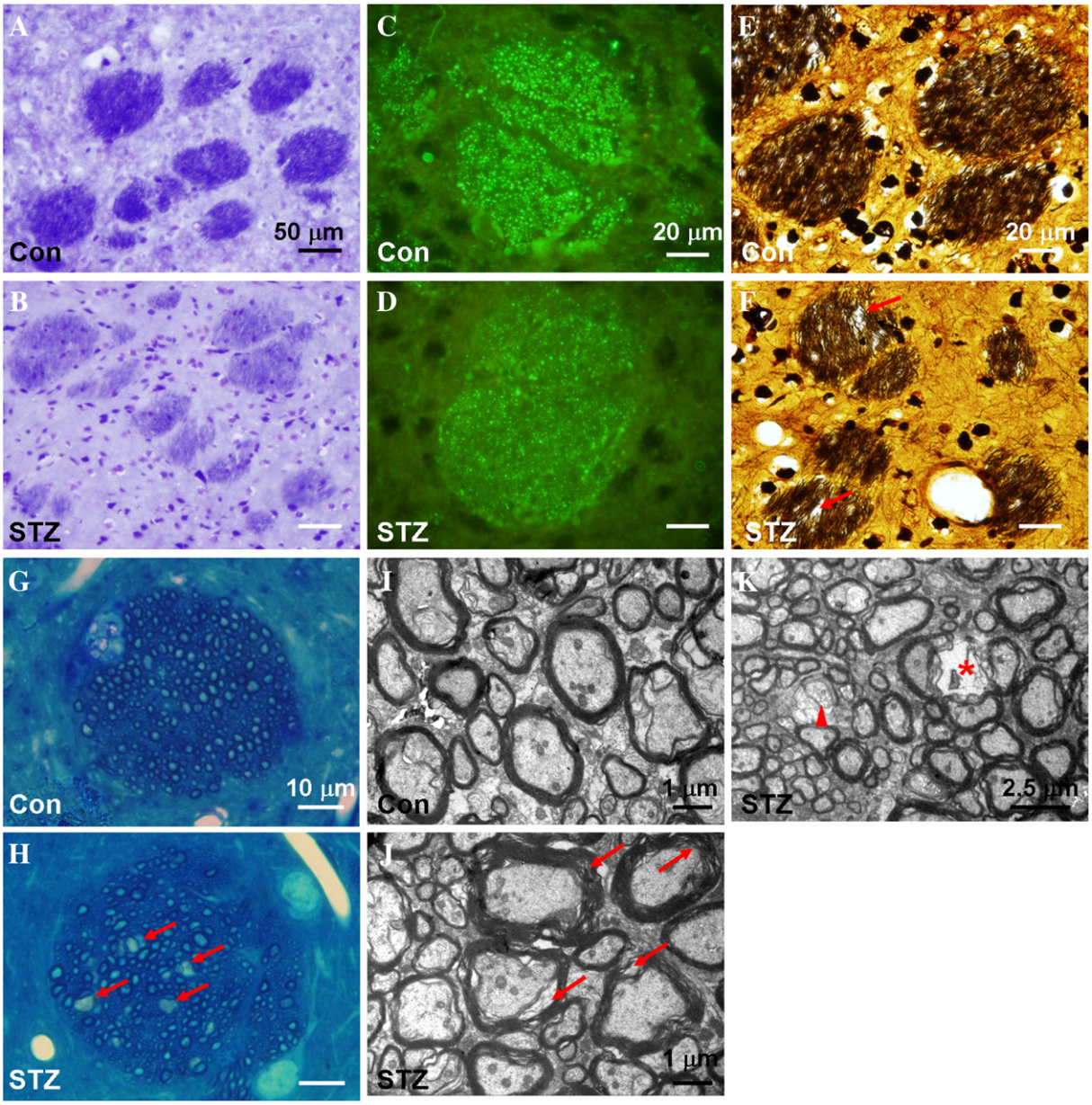

Fig. 4. Histopathological staining of the striatal sections from control rats (Con, panels A, C, E, G and I) and STZ-induced rats (STZ, panels B, D, F, H, J and K), including KB staining (A and B), SMI immunohistochemistry (C and D), BS staining (E and F), methylene blue staining (G and H) and uranyl acetate-lead citrate staining (I to K). Compared to that of the control rat, the striatal fiber bundles in the STZ-induced rats are less intensively stained with LFB (B) and SMI-31 (D), and associated with disarranged neurofibrils and vacuole formation (arrows in F and H). Ultrastructural analysis showed that the striatal fiber bundles of the STZ-induced animals are characterized by rarefied myelin sheath (arrows in J), myelin loss (arrow head in K) and signs of axonal degradation (asterisk in K).

integrity (Jeurissen et al., in press; Vos et al., 2012; Wheeler-Kingshott and Cercignani, 2009). Caution thus should be exercised in linking diabetic-induced FA, D_a and D_r changes to specific histopathological mechanisms.

In contrast to the observations in the rat model of diabetic ketoacidosis (Lam et al., 2005), we found no significant reduction of cortical apparent diffusion coefficient (ADC) in the diabetic rats (data not shown). Cerebral edema is the most common complication of diabetic ketoacidosis (Glaser et al., 2001), which may have contributed to the ADC increase observed by Lam et al. (2005). In this study, no evident signs of cerebral edema were observed in the diabetic animals.

Histological changes in diabetic striatum and cortex

The histological changes observed in the striatum and cortex of the diabetic animals are consistent with the findings from previous studies, showing that the diabetic brain is associated with demyelination and axonal injury. For example, smaller cells with reduced myelin content were found in the cortex of the STZ-induced diabetic animals at 4 weeks (Malone et al., 2006). Hernandez-Fonseca et al. showed that disarrangement of myelin sheath and oligodendrocyte abnormalities can be observed in STZ-induced rats at 8 weeks after induction (Hernandez-Fonseca et al., 2009). Reductions in myelin quantity and loss of oligodendrocytes were observed in both type 1 diabetic rats and type 2 diabetic rats at 4 months (Yang et al., 2011). In a mice model of STZ-induced type 1 diabetes, myelin loss occurred in both WM and GM regions at 8 months after induction (Francis et al., 2008). On the other hand, impairment of axonal transport in the olfactory bulbs of the STZ-induced mice occurs as early as one week after induction (Sharma et al., 2010). It was demonstrated that, after 8 weeks of hyperglycemia, the pyramidal cells in the parietal cortex, medial prefrontal cortex and hippocampus of the STZ-induced diabetic rats showed dendritic

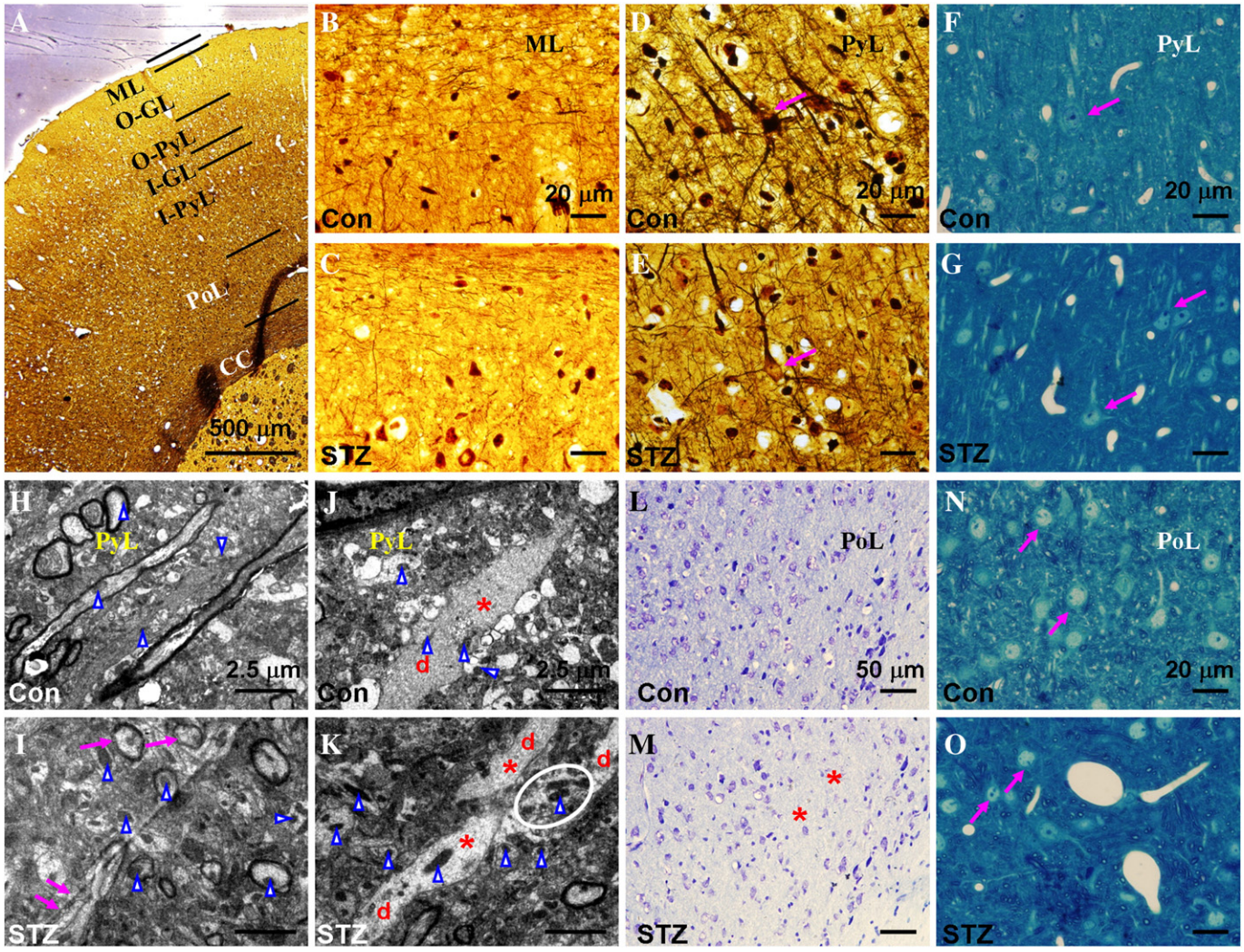

Fig. 5. Histopathological staining of the cortical sections from control rats (Con, panels B, D, F, H, J, L and N) and STZ-induced rats (STZ, panels A, C, E, G, I, K, M and O), including BS staining (A to E), methylene blue staining (F, G, N and O), uranyl acetate-lead citrate staining (H to K) and Nissl staining (L and M). Panel A illustrates the laminar structures of the cortex. The neuropil in the molecular layer of the STZ-induced rat (C) appeared to be rarefied compared to that in control (B). The arrows in D, F and N indicate normal-appearing neurons in the pyramidal layer and polymorphic layer. The arrow in E indicates the poorly BS-stained soma of a pyramidal neuron, while those in G and O indicate dystrophic neurons. The results of ultrastructural analysis were presented in H–K, in which arrowheads indicate mitochondria, the letter d indicates dendrites, and asterisks indicate neurofilaments in the dendrites. Compared to the control animals, the neurons in the pyramidal layer of the STZ-induced animals exhibited compromised integrity of the myelin sheath (arrows in I), mitochondrial abnormality (arrowheads in I and K), loss and/or fragmentation of neurofilaments in the dendrites (K), and cellular organelle aggregation (circle in K). The asterisks in M indicate regions with evident neuronal loss in the polymorphic layer. ML: molecular layer; O-GL: outer granular layer; O-PyL: outer pyramidal layer; I-GL: inner granular layer; I-PyL: inner pyramidal layer; PoL: polymorphic layer, CC: corpus callosum.

atrophy (reduced dendritic length) and reduced spine density (spine loss) (Malone et al., 2008; Martinez-Tellez et al., 2005). In their ultrastructural study on STZ-induced type 1 diabetes, Hernandez-Fonseca et al. showed that the diabetic brain is associated with degenerative changes of neurons and glia, presynaptic vesicle dispersion in swollen axonal boutons and fragmentation of neurofilaments at 8 weeks (Hernandez-Fonseca et al., 2009).

Clinical relevance of diabetes-induced cortical/striatal damage

Frontal gyrus atrophy may contribute to cognitive dysfunction (Musen et al., 2006; Wessels et al., 2006, 2007), and striatopathy may lead to movement disorders and somatosensory abnormalities in clinical diabetic patients (Abe et al., 2009). It has been suggested that diabetic brain damage are secondary to vascular complications, such as increased permeability of microvasculature, high plasma osmolality and hypoperfusion (Jakus and Rietbrock, 2004). Interestingly, the striatum and frontal cortex, the two regions most affected by STZ-treatment, are also the regions known to be especially susceptible to ischemic damage (Lei et al., 1998; Sutherland et al., 1991). In addition, the pathohistological changes in the striatum and cortex we observed in the STZ-induced rats showed resemblance to what had been reported for rats subjected to chronic cerebral hypoperfusion (Chen et al., 2011; Shibata et al., 2004). On the other hand, the presence of mitochondrial abnormalities suggests that glucose neurotoxicity could have also played a role in causing diabetic brain injuries (Edwards et al., 2010; Russell et al., 1999).

Limitations to the study

There were several limitations to this study in terms of experimental design. 1) Ketoacidosis frequently occurs in type 1 diabetic patients without glycemic control, which can cause brain damage and permanent neurological deficits (Glaser et al., 2001). In this study, the level of ketone bodies in the plasma of the diabetic rats was not monitored. Possible occurrence of ketoacidosis cannot be ruled out. However, this

is unlikely since cerebral edema, a hallmark for ketoacidosis, was not observed in our diabetic rats. 2) Most of the histology and immunohistochemistry techniques used in this study (i.e., silver staining, LFB staining and Nissl staining) are dedicated to detect demyelination and axonal/neuronal damage. More delicate and sensitive histology/immunohistochemistry techniques may reveal more subtle and specific pathological changes associated with diabetic brain damage such as synaptic loss and abnormal microglia activity (DeVisser et al., 2011; Idan-Feldman et al., 2011). 3) Given the complexity of WM configuration in the striatum and cortex, and the fact that only a limited number of animals were subjected to histology/immunohistology evaluations, no attempt was made to establish semi-quantitative correlations between the diabetes-related changes in diffusion indices and specific histopathological alterations. 4) Without glycemic control, the general conditions of the STZ-induced animals may deteriorate rapidly (Hoybergs et al., 2008). This is also the reason we performed DTI at 4 weeks after induction, but not at later time points when cognitive impairments are shown to be prominent (Idan-Feldman et al., 2011). Further studies are needed to establish whether or not changes of diffusion measures in the diabetic striatum and cortex animals are associated with cognitive/motor dysfunction. 5) Further studies on animal models of type 2 diabetes are needed, so are the studies designed to investigate the effect of glycemic control on the progress of brain complications.

There are also some limitations with respect to the image processing pipeline used in this study. First, Leemans and Jones have shown that the b-matrix needs to be adjusted during the correction of eddy currents and residual motion drifts (Leemans and Jones, 2009), and the intensity of the diffusion data has to be modulated with the Jacobian determinant due to residual phase-encoding eddy currents (Jones and Cercignani, 2010). Such steps were not performed in this study and could have potentially affected the accuracy of tensor fitting.

Second, selection of the type (i.e., isotropic vs. anisotropic) and kernel size of spatial smoothing is known to influence the VBA results on DTI data comparisons. For example, it has been an empirical rule of thumb that the FWHM should be at least twice the voxel dimension in order to get statistically robust results (Jones et al., 2005). In addition, anisotropic smoothing is known to provide better results than isotropic smoothing when performing VBA on DTI data (Van Hecke et al., 2010). In this study, we used isotropic smoothing with a Gaussian kernel having a FWHM three times the dimension of the voxel size. Anisotropic smoothing was not performed due to its technical complexity.

Finally, we used affine transformation in constructing the population-specific template and for image spatial co-registration. The use of more advanced non-rigid co-registration algorithms and tensor reorientation strategies could potentially give better results by improving the spatial and orientational alignment of the diffusion tensor images (Van Hecke et al., 2008, 2011).

Conclusion

In conclusion, we showed that, without glycemic control, the STZ-induced type 1 diabetic rats had brain injuries observable to DTI as early as 4 weeks after induction. The cerebral abnormalities associated with STZ-induced type 1 diabetes are characterized by significantly reduced FA in the motor/somatosensory cortex and striatum. The FA changes in the diabetic cortex and striatum are likely manifestations of demyelination and axonal degradation in these regions.

Acknowledgments

This work was supported by the 973 program of the Ministry of Science and Technology of China (2011CB707802) and the Natural Science Foundation of China (grants 81171302 and 20921004).

References

Abe, Y., Yamamoto, T., Soeda, T., Kumagai, T., Tanno, Y., Kubo, J., Ishihara, T., Katayama, S., 2009. Diabetic striatal disease: clinical presentation, neuroimaging, and pathology. Internal Medicine 48, 1135–1141.

Beppu, T., Inoue, T., Shibata, Y., Yamada, N., Kurose, A., Ogasawara, K., Ogawa, A., Kabasawa, H., Black, P.M., 2005. Fractional anisotropy value by diffusion tensor magnetic resonance imaging as a predictor of cell density and proliferation activity of glioblastomas. Surgical Neurology 63, 56–61.

Budde, M.D., Kim, J.H., Liang, H.F., Schmidt, R.E., Russell, J.H., Cross, A.H., Song, S.K., 2007. Toward accurate diagnosis of white matter pathology using diffusion tensor imaging. Magnetic Resonance in Medicine 57, 688–695.

Chen, J., Cui, X., Zacharek, A., Cui, Y., Roberts, C., Chopp, M., 2011. White matter damage and the effect of matrix metalloproteinases in type 2 diabetic mice after stroke. Stroke 42, 445–452.

Deboy, C.A., Zhang, J., Dike, S., Shats, I., Jones, M., Reich, D.S., Mori, S., Nguyen, T., Rothstein, B., Miller, R.H., Griffin, J.T., Kerr, D.A., Calabresi, P.A., 2007. High resolution diffusion tensor imaging of axonal damage in focal inflammatory and demyelinating lesions in rat spinal cord. Brain 130, 2199–2210.

DeVisser, A., Yang, C., Herring, A., Martinez, J.A., Rosales-Hernandez, A., Poliakov, I., Ayer, A., Garven, A., Zaver, S., Rincon, N., Xu, K.V., Tuor, U.I., Schmidt, A.M., Toth, C., 2011. Differential impact of diabetes and hypertension in the brain: adverse effects in grey matter. Neurobiology of Disease 44, 161–173.

Edwards, J.L., Quattrini, A., Lentz, S.I., Figueroa-Romero, C., Cerri, F., Backus, C., Hong, Y., Feldman, E.L., 2010. Diabetes regulates mitochondrial biogenesis and fission in mouse neurons. Diabetologia 53, 160–169.

Franc, D.T., Kodl, C.T., Mueller, B.A., Muetzel, R.L., Lim, K.O., Seaquist, E.R., 2011. High connectivity between reduced cortical thickness and disrupted white matter tracts in long-standing type 1 diabetes. Diabetes 60, 315–319.

Francis, G.J., Martinez, J.A., Liu, W.Q., Xu, K., Ayer, A., Fine, J., Tuor, U.I., Glazner, G., Hanson, L.R., Frey II, W.H., Toth, C., 2008. Intranasal insulin prevents cognitive decline, cerebral atrophy and white matter changes in murine type I diabetic encephalopathy. Brain 131, 3311–3334.

Glaser, N., Barnett, P., McCaslin, I., Nelson, D., Trainor, J., Louie, J., Kaufman, F., Quayle, K., Roback, M., Malley, R., Kuppermann, N., Amer Acad, P., 2001. Risk factors for cerebral edema in children with diabetic ketoacidosis. The New England Journal of Medicine 344, 264–269.

Hernandez-Fonseca, J.P., Rincon, J., Pedreanez, A., Viera, N., Arcaya, J.L., Carrizo, E., Mosquera, J., 2009. Structural and ultrastructural analysis of cerebral cortex, cerebellum, and hypothalamus from diabetic rats. Experimental Diabetes Research 329632, 1–12.

Hoybergs, Y.M.J.J., Biermans, R.L.V., Meert, T.F., 2008. The impact of bodyweight and body condition on behavioral testing for painful diabetic neuropathy in the streptozotocin rat model. Neuroscience Letters 436, 13–18.

Hsu, J.L., Chen, Y.L., Leu, J.G., Jaw, F.S., Lee, C.H., Tsai, Y.F., Hsu, C.Y., Bai, C.H., Leemans, A., 2012. Microstructural white matter abnormalities in type 2 diabetes mellitus: a diffusion tensor imaging study. NeuroImage 59, 1098–1105.

Hugenschmidt, C.E., Peiffer, A.M., Kraft, R.A., Casanova, R., Deibler, A.R., Burdette, J.H., Maldjian, J.A., Laurienti, P.J., 2008. Relating imaging indices of white matter integrity and volume in healthy older adults. Cerebral Cortex 18, 433–442.

Idan-Feldman, A., Schirer, Y., Polyzoidou, E., Touloumi, O., Lagoudaki, R., Grigoriadis, N.C., Gozes, I., 2011. Davunetide (NAP) as a preventative treatment for central nervous system complications in a diabetes rat model. Neurobiology of Disease 44, 327–339.

Jakus, V., Rietbrock, N., 2004. Advanced glycation end-products and the progress of diabetic vascular complications. Physiological Research 53, 131–142.

Jeurissen, B., Leemans, A., Tournier, J.D., Jones, D.K., Sijbers, J., in press. Investigating the prevalence of complex fiber configurations in white matter tissue with diffusion magnetic resonance imaging. Human Brain Mapping http://dx.doi.org/10.1002/hbm.22099.

Jones, D.K., Cercignani, M., 2010. Twenty-five pitfalls in the analysis of diffusion MRI data. NMR in Biomedicine 23, 803–820.

Jones, D.K., Symms, M.R., Cercignani, M., Howard, R.J., 2005. The effect of filter size on VBM analyses of DT-MRI data. NeuroImage 26, 546–554.

Kodl, C.T., Franc, D.T., Rao, J.P., Anderson, F.S., Thomas, W., Mueller, B.A., Lim, K.O., Seaquist, E.R., 2008. Diffusion tensor imaging identifies deficits in white matter microstructure in subjects with type 1 diabetes that correlate with reduced neurocognitive function. Diabetes 57, 3083–3089.

Lam, T.L., Anderson, S.E., Glaser, N., O'Donnell, M.E., 2005. Bumetanide reduces cerebral edema formation in rats with diabetic ketoacidosis. Diabetes 54, 510–516.

Leemans, A., Jones, D.K., 2009. The B-matrix must be rotated when correcting for subject motion in DTI data. Magnetic Resonance in Medicine 61, 1336–1349.

Lei, H., Dooley, P., Peeling, J., Corbett, D., 1998. Temporal profile of magnetic resonance imaging changes following forebrain ischemia in the gerbil. Neuroscience Letters 257, 105–108.

Malone, J.I., Hanna, S.K., Saporta, S., 2006. Hyperglycemic brain injury in the rat. Brain Research 1076, 9–15.

Malone, J.I., Hanna, S., Saporta, S., Mervis, R.F., Park, C.R., Chong, L., Diamond, D.M., 2008. Hyperglycemia not hypoglycemia alters neuronal dendrites and impairs spatial memory. Pediatric Diabetes 9, 531–539.

Martinez-Tellez, R., Gomez-Villalobos, M.D.J., Flores, G., 2005. Alteration in dendritic morphology of cortical neurons in rats with diabetes mellitus induced by streptozotocin. Brain Research 1048, 108–115.

Mukherjee, P., Miller, J.H., Shimony, J.S., Philip, J.V., Nehra, D., Snyder, A.Z., Conturo, T.E., Neil, J.J., McKinstry, R.C., 2002. Diffusion-tensor MR imaging of gray and white matter development during normal human brain maturation. AJNR. American Journal of Neuroradiology 23, 1445–1456.

Musen, G., Lyoo, I.K., Sparks, C.R., Weinger, K., Hwang, J., Ryan, C.M., Jimerson, D.C., Hennen, J., Renshaw, P.F., Jacobson, A.M., 2006. Effects of type 1 diabetes on gray matter density as measured by voxel-based morphometry. Diabetes 55, 326–333.
Neil, J.J., Shiran, S.I., McKinstry, R.C., Schefft, G.L., Snyder, A.Z., Almli, C.R., Akbudak, E., Aronovitz, J.A., Miller, J.P., Lee, B.C.P., Conturo, T.E., 1998. Normal brain in human newborns: apparent diffusion coefficient and diffusion anisotropy measured by using diffusion tensor MR imaging. Radiology 209, 57–66.
Russell, J.W., Sullivan, K.A., Windebank, A.J., Herrmann, D.N., Feldman, E.L., 1999. Neurons undergo apoptosis in animal and cell culture models of diabetes. Neurobiology of Disease 6, 347–363.
Shan, D.E., Ho, D.M.T., Chang, C., Pan, H.C., Teng, M.M.H., 1998. Hemichorea–hemiballism: an explanation for MR signal changes. AJNR. American Journal of Neuroradiology 19, 863–870.
Sharma, R., Buras, E., Terashima, T., Serrano, F., Massaad, C.A., Hu, L., Bitner, B., Inoue, T., Chan, L., Pautler, R.G., 2010. Hyperglycemia induces oxidative stress and impairs axonal transport rates in mice. PLoS One 5, e13463.
Shibata, M., Ohtani, R., Ihara, M., Tomimoto, H., 2004. White matter lesions and glial õactivation in a novel mouse model of chronic cerebral hypoperfusion. Stroke 35, 2598–2603.
Smith, S.M., Jenkinson, M., Johansen-Berg, H., Rueckert, D., Nichols, T.E., Mackay, C.E., Watkins, K.E., Ciccarelli, O., Cader, M.Z., Matthews, P.M., Behrens, T.E.J., 2006. Tract-based spatial statistics: voxelwise analysis of multi-subject diffusion data. NeuroImage 31, 1487–1505.
Song, S.K., Sun, S.W., Ramsbottom, M.J., Chang, C., Russell, J., Cross, A.H., 2002. Dysmyelination revealed through MRI as increased radial (but unchanged axial) diffusion of water. NeuroImage 17, 1429–1436.
Song, S.K., Yoshino, J., Le, T.Q., Lin, S.J., Sun, S.W., Cross, A.H., Armstrong, R.C., 2005. Demyelination increases radial diffusivity in corpus callosum of mouse brain. NeuroImage 26, 132–140.
Sun, S.W., Liang, H.F., Trinkaus, K., Cross, A.H., Armstrong, R.C., Song, S.K., 2006. Noninvasive detection of cuprizone induced axonal damage and demyelination in the mouse corpus callosum. Magnetic Resonance in Medicine 55, 302–308.
Sutherland, G.R., Peeling, J., Lesiuk, H.J., Brownstone, R.M., Rydzy, M., Saunders, J.K., Geiger, J.D., 1991. The effects of caffeine on ischemic neuronal injury as determined by magnetic-resonance-imaging and histopathology. Neuroscience 42, 171–182.
Tournier, J.D., Mori, S., Leemans, A., 2011. Diffusion tensor imaging and beyond. Magnetic Resonance in Medicine 65, 1532–1556.
van Elderen, S.G.C., de Roos, A., de Craen, A.J.M., Westendorp, R.G.J., Blauw, G.J., Jukema, J.W., Bollen, E.L.E.M., Middelkoop, H.A.M., van Buchem, M.A., van der Grond, J., 2010. Progression of brain atrophy and cognitive decline in diabetes mellitus. Neurology 75, 997–1002.
van Harten, B., de Leeuw, F.-E., Weinstein, H.C., Scheltens, P., Biessels, G.J., 2006. Brain imaging in patients with diabetes — a systematic review. Diabetes Care 29, 2539–2548.
Van Hecke, W., Sijbers, J., D'Agostino, E., Maes, F., De Backer, S., Vandervliet, E., Parizel, P.M., Leemans, A., 2008. On the construction of an inter-subject diffusion tensor magnetic resonance atlas of the healthy human brain. NeuroImage 43, 69–80.
Van Hecke, W., Leemans, A., De Backer, S., Jeurissen, B., Parizel, P.M., Sijbers, J., 2010. Comparing isotropic and anisotropic smoothing for voxel-based DTI analyses: a simulation study. Human Brain Mapping 31, 98–114.
Van Hecke, W., Leemans, A., Sage, C.A., Emsell, L., Veraart, J., Sijbers, J., Sunaert, S., Parizel, P.M., 2011. The effect of template selection on diffusion tensor voxel-based analysis results. NeuroImage 55, 566–573.
Vos, S.B., Jones, D.K., Jeurissen, B., Viergever, M.A., Leemans, A., 2012. The influence of complex white matter architecture on the mean diffusivity in diffusion tensor MRI of the human brain. NeuroImage 59, 2208–2216.
Wessels, A.M., Simsek, S., Remijnse, P.L., Veltman, D.J., Biessels, G.J., Barkhof, F., Scheltens, P., Snoek, F.J., Heine, R.J., Rombouts, S.A.R.B., 2006. Voxel-based morphometry demonstrates reduced grey matter density on brain MRI in patients with diabetic retinopathy. Diabetologia 49, 2474–2480.
Wessels, A.M., Rombouts, S.A.R.B., Remijnse, P.L., Boom, Y., Scheltens, P., Barkhof, F., Heine, R.J., Snoek, F.J., 2007. Cognitive performance in type 1 diabetes patients is associated with cerebral white matter volume. Diabetologia 50, 1763–1769.
Wheeler-Kingshott, C.A.M., Cercignani, M., 2009. About "axial" and "radial" diffusivities. Magnetic Resonance in Medicine 61, 1255–1260.
Wu, Q.Z., Butzkueven, H., Gresle, M., Kirchhoff, F., Friedhuber, A., Yang, Q., Wang, H., Fang, K., Lei, H., Egan, G.F., Kilpatrick, T.J., 2007. MR diffusion changes correlate with ultrastructurally defined axonal degeneration in murine optic nerve. NeuroImage 37, 1138–1147.
Yang, C., DeVisser, A., Martinez, J.A., Poliakov, I., Rosales-Hernandez, A., Ayer, A., Garven, A., Zaver, S., Rincon, N., Xu, K., Tuor, U.I., Schmidt, A.M., Toth, C., 2011. Differential impact of diabetes and hypertension in the brain: adverse effects in white matter. Neurobiology of Disease 42, 446–458.
Yau, P.L., Javier, D., Tsui, W., Sweat, V., Bruehl, H., Borod, J.C., Convit, A., 2009. Emotional and neutral declarative memory impairments and associated white matter microstructural abnormalities in adults with type 2 diabetes. Psychiatry Research 174, 223–230.
Yu, C.S., Lin, F.C., Li, K.C., Jiang, T.Z., Zhu, C.Z., Qin, W., Sun, H., Chan, P., 2006. Diffusion tensor imaging in the assessment of normal-appearing brain tissue damage in relapsing neuromyelitis optica. AJNR. American Journal of Neuroradiology 27, 1009–1015.